

Extreme THz fields from two-color filamentation of mid-infrared laser pulses

Vladimir Yu. Fedorov^{1,2} and Stelios Tzortzakis^{1,3,4}

¹Science Program, Texas A&M University at Qatar, P.O. Box 23874, Doha, Qatar

²P. N. Lebedev Physical Institute of the Russian Academy of Sciences,

53 Leninskiy Prospekt, 119991, Moscow, Russia*

³Institute of Electronic Structure and Laser (IESL),

Foundation for Research and Technology - Hellas (FORTH), P.O. Box 1527, GR-71110 Heraklion, Greece

⁴Materials Science and Technology Department, University of Crete, 71003, Heraklion, Greece[†]

(Dated: August 25, 2017)

Nonlinear THz photonics is probably the last frontier of nonlinear optics. The strength of both the electric and the magnetic fields of these ultrashort low frequency light bunches opens the way to exciting science and applications. Progress in the field though is slow because of the deficiency in suitable sources. Here we show that two-color filamentation of mid-infrared $3.9\ \mu\text{m}$ laser pulses allows one to generate single cycle THz pulses with multi-millijoule energies and extreme conversion efficiencies. Moreover, the focused THz peak electric and magnetic fields reach values of GV/cm and kT, respectively, exceeding by far any available quasi-DC field source today. These fields enable extreme field science, including into other, relativistic phenomena. Besides, we elucidate the origin of this high efficiency, which is made up of several factors, including a novel mechanism where the harmonics produced by the mid-infrared pulses strongly contribute to the field symmetry breaking and enhance the THz generation.

Introduction.—The terahertz (THz) frequency range (0.1-10 THz) is a part of the electromagnetic spectrum located at the junction between the microwave and optical frequencies. For many reasons THz frequencies attract a lot of interest in recent years [1, 2]. Since structural absorption resonances of many molecules belong to the THz frequency band, THz spectroscopy becomes a unique tool for matter studies. Moreover, THz frequencies lie at the boundary of frequency ranges that are characteristic for high-frequency electronics and photonics. Therefore, THz devices are expected to be a connecting link between these technologies. In addition, THz radiation penetrates through a variety of non-conducting materials like clothing, paper, wood, masonry, plastic and ceramics. But unlike X-rays, THz radiation is not an ionizing radiation and does not damage test materials, which opens great opportunities for its application in industrial quality control, homeland security, or medical diagnostics and treatment.

Although the THz frequency range has very rich scientific and technological potential, it remains underexplored due to lack of intense THz sources and sensitive THz detectors. The progressive appearance of suitable bright THz sources opens a new era for studies of extreme THz field-matter interactions, nonlinear THz spectroscopy and imaging. To date, there are two major techniques for the generation of intense THz pulses on tabletop setups [3, 4]: optical rectification in nonlinear crystals [5–7] and two-color filamentation (photoionization of gases by dual-frequency laser fields) [8–10]. Optical rectification has THz conversion efficiencies (ratio of generated THz energy to energy of input laser pulse) that can reach 3.7% [5]. Nevertheless, the spectral bandwidth of these sources is limited to frequencies below 5 THz and the generated THz pulses energies are also limited, be-

cause of the damage threshold of the crystals, with the highest energy reported to date reaching 0.9 mJ [6]. In turn, two-color filamentation presents lower THz conversion efficiencies ($\sim 0.01\%$) and produces less intense THz pulses with energies up to $30\ \mu\text{J}$ [8–10]. However, THz pulses generated by two-color filamentation have much larger spectral bandwidths ($> 50\ \text{THz}$) and can be generated at remote distances [11–13], which allows to overcome a number of THz propagation issues, such as high absorption in atmospheric water vapor and diffraction.

Up to date, most experiments on two-color filamentation were conducted using Titanium:Sapphire (Ti:Sa) laser sources with central wavelength around $0.8\ \mu\text{m}$ and their second harmonic. A study using longer wavelengths, in the near infrared, showed an enhancement of the THz conversion efficiency with increasing pump wavelength but only up to $1.8\ \mu\text{m}$, while beyond this point the efficiency dropped again [14]. Also, a theoretical study showed stronger THz generation compared to $0.8\ \mu\text{m}$ using single color mid-infrared pulses with Particle in Cell (PIC) simulations, not considering though nonlinear propagation effects [15]. Recently though, filamentation of mid-infrared (mid-IR) laser pulses with $3.9\ \mu\text{m}$ central wavelength was for the first time demonstrated experimentally [16]. The subsequent experimental and theoretical studies revealed that compared to $0.8\ \mu\text{m}$ laser pulses, filaments produced by $3.9\ \mu\text{m}$ are longer with wider plasma channels and the generated supercontinuum is extremely broad ranging up to harmonics of 15th order [16–21].

In this work we study numerically the generation of THz radiation by two-color filamentation of $3.9\ \mu\text{m}$ laser pulses. We show that compared to $0.8\ \mu\text{m}$ pulses, the THz conversion efficiency in mid-IR filaments is two orders of magnitude higher, the energy of the gener-

ated THz pulses reaches the multi-millijoule level, and the strength of the THz fields can reach the GV/cm range. Thus, two-color filamentation of mid-IR laser pulses emerges as the ultimate source for extreme THz science since it allows one to generate THz radiation with unprecedented efficiency and extremely high energy that largely overcomes all other approaches while energy scaling does not suffer from undesired effects like damage of crystals in the optical rectification.

Model.—To simulate the two-color filamentation of mid-IR laser pulses in air we use the Unidirectional Pulse Propagation Equation (UPPE) [22, 23] coupled with the kinetic equation for plasma concentration [24] (see the Supplemental Material [25]). This model takes into account nonparaxial propagation of polychromatic fields without any kind of envelope approximations. It includes dispersion of all orders, cubic Kerr nonlinearity, defocusing in plasma, inverse Bremsstrahlung, photoionization with corresponding energy losses, and avalanche ionization. We use a realistic dispersion model of dry atmospheric air (zero relative humidity) that takes into account spectral lines of N_2 , O_2 , and CO_2 gases from the HITRAN database [26].

Our initial condition for the UPPE equation is the following two-color field E :

$$E = \exp\left(-\frac{r^2}{2a_0^2} - \frac{t^2}{2\tau_0^2}\right) [E_1 \cos(\omega_0 t) + E_2 \cos(2\omega_0 t)],$$

where $r^2 = x^2 + y^2$, $a_0 = 4/2\sqrt{\log 2}$ mm is the beam size (4 mm FWHM), $\tau_0 = 100/2\sqrt{\log 2}$ fs is the pulse duration (100 fs FWHM), ω_0 is the central frequency, while E_1 and E_2 being the amplitudes of the fundamental and second harmonic pulses, respectively. The initial pulse is focused by a lens with a focal distance $f = 200$ mm. To simulate the focusing we multiplied each Fourier harmonic of the field E by a factor $\exp[-i(\omega/c_0)r^2/(2f)]$, where ω is the frequency of the corresponding harmonic and c_0 is the speed of light in vacuum. In our simulations the central wavelength λ_0 of the fundamental pulse is equal to $3.9 \mu\text{m}$. Also, in order to have a reference for comparison we simulated two-color filamentation of the same laser pulse but with $\lambda_0 = 0.8 \mu\text{m}$. The energy W of the initial two-color pulse is equal to 29 mJ for $\lambda_0=3.9 \mu\text{m}$ and 1.23 mJ for $\lambda_0=0.8 \mu\text{m}$. For both cases the fundamental and second harmonic pulses hold, respectively, 95% and 5% of this energy. The energy W for each wavelength was chosen in such a way that the power of the corresponding single-color pulse at wavelength λ_0 is equal, in both cases, to $1.2P_{cr}$, where P_{cr} is the critical power of self-focusing in air at this wavelength.

Results.—Using the above model we numerically simulated the two-color filamentation of $3.9 \mu\text{m}$ and $0.8 \mu\text{m}$ pulses in air. Figure 1 shows the dependence of several filamentation integral parameters on propagation distance for both wavelengths. One can see that the peak intensity, peak fluence, and peak plasma concentration in the

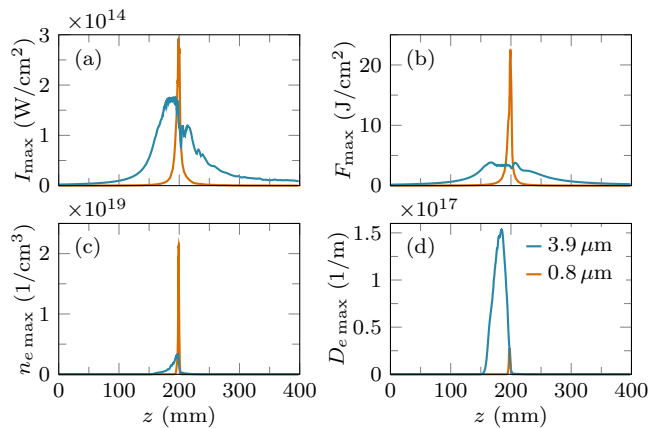


FIG. 1. (a) Peak intensity I_{\max} , (b) peak fluence F_{\max} , (c) peak plasma concentration $n_{e \max}$, and (d) plasma concentration integrated over radius, $D_{e \max}$, versus propagation distance z for the $3.9 \mu\text{m}$ and the $0.8 \mu\text{m}$ two-color laser pulses.

case of $3.9 \mu\text{m}$ pulse are several times lower than for the $0.8 \mu\text{m}$ pulse. However, the filament produced by the $3.9 \mu\text{m}$ pulse is about 3 times longer. Moreover, much higher integrated over radius plasma concentration shows that the plasma channel produced by the $3.9 \mu\text{m}$ pulse is considerably wider compared to the $0.8 \mu\text{m}$ pulse.

Figure 2 shows the dependence of the integrated power spectrum S on propagation distance z and frequency f for the two wavelengths. One can see that filamentation of $3.9 \mu\text{m}$ two-color pulse is accompanied by generation of extremely broad supercontinuum, which includes all even and odd harmonics up to at least the 15th order. Though the most intriguing result is the impressive energy transferred to the THz part of the spectrum with the $3.9 \mu\text{m}$ pulses compared to the case of the $0.8 \mu\text{m}$ ones. The THz conversion efficiency (for frequencies f lying below 40 THz) for $0.8 \mu\text{m}$ pulses is 0.06%, while the one for $3.9 \mu\text{m}$ pulses is 6.7%, that is more than two orders of magnitude higher. Note that this conversion efficiency is the highest reported to date compared to any of the known approaches for THz generation.

Figure 3a shows how the energy of the THz pulse generated during two-color filamentation of $3.9 \mu\text{m}$ pulses depends on the propagation distance z . One can see that close to the end of the filament ($z \simeq 220$ mm) the energy of the THz pulse reaches almost 2 mJ. Note that the decrease of the THz energy at longer propagation distances is purely numerical and is due to losses of the diffracting THz beam in the absorbing boundary layers located at the end of the numerical grid. In turn, the peak THz energy generated by $0.8 \mu\text{m}$ pulses is only about $0.8 \mu\text{J}$. In other words, the THz pulse generated by the $3.9 \mu\text{m}$ pulse is 2500 times (three orders of magnitude!) more energetic than the one generated by $0.8 \mu\text{m}$ pulses.

Figure 3b shows the on-axis THz electric field generated by $3.9 \mu\text{m}$ pulses at a distance $z = 190$ mm (in

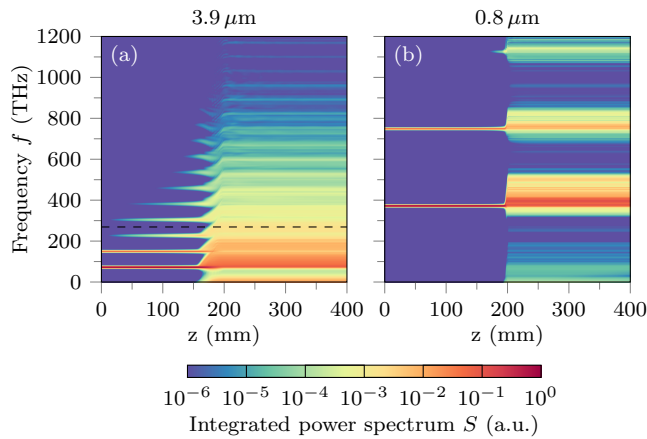


FIG. 2. Dependence of integrated pulse power spectrum S on propagation distance z and frequency f for $3.9\ \mu\text{m}$ (a) and $0.8\ \mu\text{m}$ (b) two-color laser pulses. The black dashed line separates the harmonics of 4th order and higher.

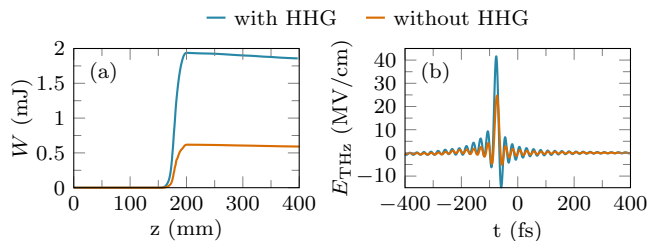


FIG. 3. (a) Energy of THz pulse W versus propagation distance z . (b) THz electric field versus time t at $z = 190\ \text{mm}$. THz pulses are generated during two-color filamentation of $3.9\ \mu\text{m}$ pulses in the case of air with (cyan) or without (orange) high harmonics generation.

the middle of the filament). One can see that the field strength (the amplitude from minimum to maximum of the field) of the generated THz pulse reaches $56\ \text{MV}/\text{cm}$, which exceeds the field strengths obtained in the most efficient experiments with optical rectification [6].

Figure 4 shows the angularly-resolved frequency spectrum of the THz pulse generated during two-color filamentation of $3.9\ \mu\text{m}$ and $0.8\ \mu\text{m}$ pulses. One can see that in both cases the THz radiation is emitted into a cone, where higher frequencies propagate at smaller angles. Also, we see that in average the angle of the THz emission cone is smaller in the case of $\lambda_0 = 3.9\ \mu\text{m}$ ($\sim 7^\circ$ for $0.8\ \mu\text{m}$ and $\sim 2^\circ$ for $3.9\ \mu\text{m}$ pulses). Thus, an extra advantage of the THz radiation produced during two-color filamentation of $3.9\ \mu\text{m}$ is its better directionality compared to the case of $0.8\ \mu\text{m}$ pulses.

Discussion.—As we have already seen two-color filamentation of mid-IR laser pulses allows one to generate THz pulses of very high energy and field strength. High efficiency of THz generation by mid-IR two-color pulses is made up of several factors. Maybe the most intriguing of them is related to the highly efficient generation of high

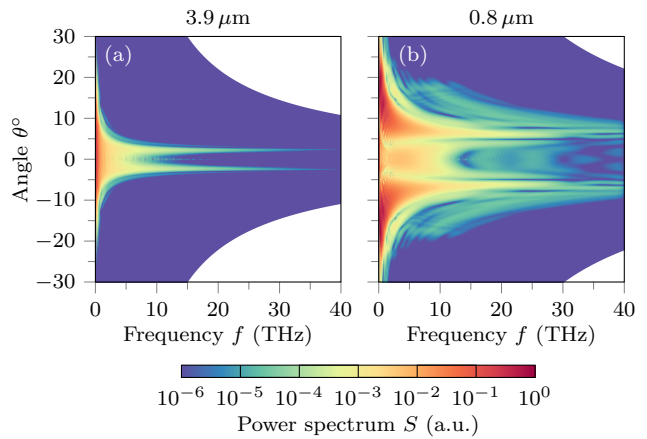


FIG. 4. Dependence of pulse power spectrum S on frequency f and angle θ for $3.9\ \mu\text{m}$ (a) and $0.8\ \mu\text{m}$ (b) two-color laser pulses at distance $z = 220\ \text{mm}$.

harmonics during mid-IR filamentation. In Fig. 2 we see that the spectrum produced by $3.9\ \mu\text{m}$ pulses consists of all harmonics, both even and odd, up to the 15th order. Thus, filamentation of two-color $3.9\ \mu\text{m}$ pulses is accompanied by generation of a multiple number of secondary dual frequency pulses ($2\omega-4\omega$, $3\omega-6\omega$, $4\omega-8\omega$, etc.). Each of these secondary pulses contribute to the field symmetry breaking and support further THz generation. In order to test this hypothesis, we repeated the simulations of two-color filamentation with $3.9\ \mu\text{m}$ pulses, but during these simulations at each propagation step we filtered out all harmonics of order 4 and higher (the black dashed line in Fig. 2 shows the boundary of the spectral filter). The energy and the electric field of the THz pulses obtained from these simulations are plotted in Fig. 3. One can see that without higher harmonics the energy of the generated THz pulse drops down by 3 times.

In addition, mid-IR laser pulses produce much stronger photocurrents compared to $0.8\ \mu\text{m}$ pulses. This can be seen from the following estimations. The velocity v of a free electron under the action of the Lorentz force produced by a monochromatic field of amplitude A and frequency ω_0 is given by the equation $dv/dt = q_e/m_e A \cos(\omega_0 t)$, where q_e and m_e are the charge and mass of electron, respectively. After integration we find $v = (q_e/m_e)(A/\omega_0) \sin(\omega_0 t)$ (the initial velocity of free electrons after ionization is assumed to be zero). Therefore the average electron velocity $\sqrt{v^2} = (q_e/m_e)(A/2\omega_0)$ is proportional to the wavelength $\lambda_0 = 2\pi c_0/\omega_0$. Thus, the photocurrent $J = q_e v$ produced by $3.9\ \mu\text{m}$ pulses and, as a consequence the generated THz field, is about five times stronger compared to $0.8\ \mu\text{m}$ pulses.

Another factor contributing to the highly efficient THz generation is a smaller walk-off between the fundamental and the second harmonic. According to our dispersion model (see the Supplemental Material [25]) the walk-off between $0.4\ \mu\text{m}$ and $0.8\ \mu\text{m}$ pulses is $81\ \text{fs}/\text{m}$. In turn

the walk-off between $1.95\ \mu\text{m}$ and $3.9\ \mu\text{m}$ pulses is only $1.26\ \text{fs/m}$ for air with CO_2 and $3.04\ \text{fs/m}$ for air without CO_2 . That is, the walk-off for $3.9\ \mu\text{m}$ two-color pulses is at least 20 times less than for $0.8\ \mu\text{m}$ pulses. In turn, keeping in mind the Cherenkov mechanism of THz generation [27], smaller walk-off between the THz and fundamental pulses explains the better directionality of THz radiation in the case of mid-IR pulses (see Fig. 4).

Besides, the THz generation efficiency is higher for $3.9\ \mu\text{m}$ two-color pulses because it produces ~ 3 times longer plasma channels that contain ~ 45 times more free electrons (see Fig. 1).

It is interesting that in our studies we did not reveal any effect of the CO_2 gas on THz generation efficiency, as one could suggest because of the absorption line near the $3.9\ \mu\text{m}$ and the corresponding anomalous dispersion (see the Supplemental Material [25]). For air with and without CO_2 the results of our simulations are so close that it is very hard to see any difference on any of the above figures.

To sum up, the much higher efficiency of THz generation by $3.9\ \mu\text{m}$ two-color pulses compared to $0.8\ \mu\text{m}$ ones can be explained by the extra field symmetry breaking due to higher harmonics, the 5 times stronger photocurrents, the tens of times smaller walk-off between the fundamental and its second harmonic, the 3 times longer plasma channels, and the 45 times more total free electrons.

In addition, we studied how the parameters of generated THz radiation scale with the input energy W of the $3.9\ \mu\text{m}$ two-color pulses. Figure 5a shows that the energy of the generated THz pulse grows almost linearly with energy W , reaching $15\ \text{mJ}$ at $W = 232\ \text{mJ}$. The THz conversion efficiency weakly depends on input energy and is about 7% (see Fig. 5b). The peak THz electric field strengths obtained for $W=29, 58, 116,$ and $232\ \text{mJ}$ are equal to $56, 65, 67,$ and $77\ \text{MV/cm}$, respectively. Considering the almost linear increase of the THz energy with increasing W , and taking into account that the width of the THz spectrum remains the same, this rather small growth of THz field strength suggests that the spatial size of the generated THz pulses increases with W . To verify this, we calculated the fluence distributions (intensities integrated over time) for all THz pulses and estimated their $1/e$ radii a_{THz} using a Gaussian fitting. As a result we obtained $a_{\text{THz}}=0.5, 0.77, 1.72,$ and $2.2\ \text{mm}$ for the corresponding input energies $W=29, 58, 116,$ and $232\ \text{mJ}$. Thus, the growth of THz energy with increase of the input laser energy happens mainly due to increase of the THz beam spatial size.

Although the obtained THz field strengths already exceed the highest values reported in the literature, one can reach even higher values when focusing the corresponding THz beams. As a simple estimate, we recall that for Gaussian beams the field at the focus of a lens with focal distance f is L_d/f times higher than the ini-

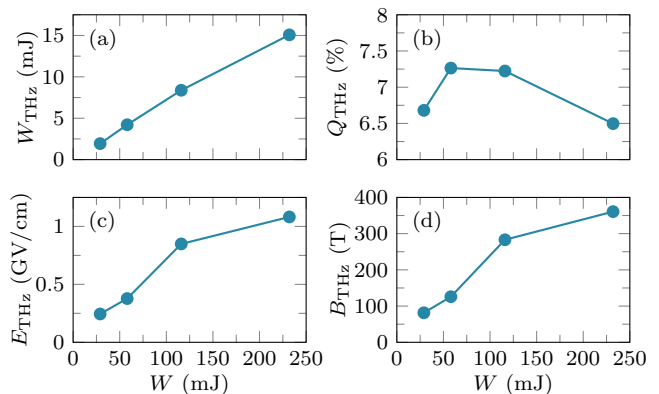


FIG. 5. (a) THz pulse energy W_{THz} , (b) THz conversion efficiency Q_{THz} , (c) estimated peak electric field E_{THz} of focused THz pulse, and (d) estimated peak magnetic field B_{THz} of focused THz pulse versus input energy W of $3.9\ \mu\text{m}$ two-color laser pulses.

tial one. Here $L_d = 2\pi f_0/c_0 a_0^2$ is the diffraction length, where f_0 is the central frequency and a_0 is the $1/e$ beam radius. We apply this estimate for our THz pulses using the previously calculated radii a_{THz} and $f_0=8\ \text{THz}$. This central frequency corresponds to the center of mass of the THz power spectrum (we found that f_0 does not change with W). Figure 5c shows that the estimated THz field strengths E_{THz} in the focus of a $1''$ off-axis parabolic mirror ($f=25.4\ \text{mm}$) reach the GV/cm level ($1.1\ \text{GV/cm}$ for $W=232\ \text{mJ}$). In turn, the corresponding magnetic fields $B_{\text{THz}} = E_{\text{THz}}/c_0$ reach several hundreds of tesla (see Fig. 5d).

Note that the above estimates are quite relaxed, for the $W=232\ \text{mJ}$ case, for example, the above focusing conditions produce a THz focal waist that is about 2.8 times the central THz wavelength. This means that one could achieve even stronger focusing, like for instance in [7]. This in turn would result in magnetic fields that go beyond the kT regime, exceeding any laboratory produced quasi-DC magnetic field reported to date by any means.

Conclusions.—In conclusion, we numerically simulated two-color filamentation of $3.9\ \mu\text{m}$ laser pulses in realistic atmospheric pressure air. We have shown, that compared to the case of $0.8\ \mu\text{m}$ pulses, THz generation efficiency by $3.9\ \mu\text{m}$ two-color pulses is two orders of magnitude higher. The energy of THz radiation generated by $3.9\ \mu\text{m}$ two-color pulses reaches the multi-millijoule level, the THz electric field strengths can go beyond the GV/cm level and the magnetic fields can reach the kT. Such high THz efficiency and energy of THz pulses generated by mid-IR pulses is the result of several factors, including a novel mechanism where generated high harmonics contribute to the field symmetry breaking. The other factors are stronger photocurrents, negligible walk-offs between harmonics, longer and wider plasma channels. As a result, we have shown that two-color filamen-

tation of mid-IR laser pulses, being a source of extremely bright THz radiation, can open the way for future studies of extreme THz field-matter interactions, nonlinear THz spectroscopy and imaging.

This work was supported by the National Priorities Research Program grant No. NPRP9-383-1-083 from the Qatar National Research Fund (member of The Qatar Foundation) and the European Unions Horizon 2020 Laserlab Europe (EC-GA 654148).

* v.y.fedorov@gmail.com

† stzortz@iesl.forth.gr

- [1] X. C. Zhang, A. Shkurinov, and Y. Zhang, *Nature Photonics* **11**, 16 (2017).
- [2] M. Tonouchi, *Nature Photonics* **1**, 97 (2007).
- [3] R. A. Lewis, *Journal of Physics D: Applied Physics* **47**, 374001 (2014).
- [4] K. Reimann, *Reports on Progress in Physics* **70**, 1597 (2007).
- [5] W. R. Huang, S.-W. Huang, E. Granados, K. Ravi, K.-H. Hong, L. E. Zapata, and F. X. Kärtner, *Journal of Modern Optics* **62**, 1 (2014).
- [6] C. Vicario, A. V. Ovchinnikov, S. I. Ashitkov, M. B. Agranat, V. E. Fortov, and C. P. Hauri, *Optics Letters* **39**, 6632 (2014).
- [7] M. Shalaby and C. P. Hauri, *Nature Communications* **6**, 1 (2015).
- [8] K. Y. Kim, A. J. Taylor, J. H. Glowina, and G. Rodriguez, *Nature Photonics* **2**, 605 (2008).
- [9] T. I. Oh, Y. J. Yoo, Y. S. You, and K. Y. Kim, *Applied Physics Letters* **105**, 041103 (2014).
- [10] D. Kuk, Y. J. Yoo, E. W. Rosenthal, N. Jhajj, H. M. Milchberg, and K. Y. Kim, *Applied Physics Letters* **108**, 121106 (2016).
- [11] T. J. Wang, S. Yuan, Y. Chen, J. F. Daigle, C. Marceau, F. Théberge, M. Châteauneuf, J. Dubois, and S. L. Chin, *Applied Physics Letters* **97**, 111108 (2010).
- [12] T. J. Wang, J. F. Daigle, S. Yuan, F. Théberge, M. Châteauneuf, J. Dubois, G. Roy, H. Zeng, and S. L. Chin, *Physical Review A* **83**, 053801 (2011).
- [13] J.-F. Daigle, F. Théberge, M. Henriksson, T.-J. J. Wang, S. Yuan, M. Châteauneuf, J. Dubois, M. Piché, and S. L. Chin, *Optics Express* **20**, 6825 (2012).
- [14] M. Clerici, M. Peccianti, B. E. Schmidt, L. Caspani, M. Shalaby, M. Giguère, A. Lotti, A. Couairon, F. Légaré, T. Ozaki, D. Faccio, and R. Morandotti, *Physical Review Letters* **110**, 253901 (2013).
- [15] W.-M. Wang, S. Kawata, Z.-M. Sheng, Y.-T. Li, L.-M. Chen, L.-J. Qian, and J. Zhang, *Optics Letters* **36**, 2608 (2011).
- [16] A. V. Mitrofanov, A. A. Voronin, D. A. Sidorov-Biryukov, A. Pugžlys, E. A. Stepanov, G. Andriukaitis, T. Flöry, S. Ališauskas, A. B. Fedotov, A. Baltuška, and A. M. Zheltikov, *Scientific Reports* **5**, 8368 (2015).
- [17] P. Panagiotopoulos, P. Whalen, M. Kolesik, and J. V. Moloney, *Nature Photonics* **9**, 543 (2015).
- [18] A. V. Mitrofanov, A. A. Voronin, D. A. Sidorov-Biryukov, S. I. Mitryukovsky, A. B. Fedotov, E. E. Serebryannikov, D. V. Meshchankin, V. Shumakova, S. Al-

isauskas, A. Pugžlys, V. Y. Panchenko, A. Baltuška, and A. M. Zheltikov, *Optica* **3**, 299 (2016).

- [19] A. V. Mitrofanov, A. A. Voronin, D. A. Sidorov-Biryukov, S. I. Mitryukovsky, M. V. Rozhko, A. Pugžlys, A. B. Fedotov, V. Y. Panchenko, A. Baltuska, and A. M. Zheltikov, *Optics Letters* **41**, 3479 (2016).
- [20] P. Panagiotopoulos, M. Kolesik, and J. V. Moloney, *Physical Review A* **94**, 033852 (2016).
- [21] N. A. Panov, D. E. Shipilo, V. A. Andreeva, O. G. Kosareva, A. M. Saletsky, H. Xu, and P. Polynkin, *Physical Review A* **94**, 041801 (2016).
- [22] M. Kolesik, J. V. Moloney, and M. Mlejnek, *Physical Review Letters* **89**, 283902 (2002).
- [23] M. Kolesik and J. V. Moloney, *Physical Review E* **70**, 036604 (2004).
- [24] A. Couairon, E. Brambilla, T. Corti, D. Majus, O. Ramírez-Góngora, and M. Kolesik, *The European Physical Journal Special Topics* **199**, 5 (2011).
- [25] “See Supplemental Material at XXX for the details on model used in our simulations.”
- [26] “HITRAN on the Web,” <http://hitran.iao.ru/>, accessed: 2017-07-05.
- [27] L. A. Johnson, J. P. Palastro, T. M. Antonsen, and K. Y. Kim, *Physical Review A* **88**, 063804 (2013).
- [28] A. M. Perelomov, V. S. Popov, and M. V. Terent’ev, *Soviet Physics JETP* **24**, 207 (1967).
- [29] E. R. Peck and K. Reeder, *Journal of the Optical Society of America* **62**, 958 (1972).

SUPPLEMENTAL MATERIAL

In our simulations we use the Unidirectional Pulse Propagation Equation (UPPE) [22–24], given by:

$$\frac{\partial \hat{E}}{\partial z} = ik_z \hat{E} + i \frac{\mu_0 \mu \omega^2}{2k_z} \hat{N}, \quad (1)$$

where $\hat{E}(k_x, k_y, \omega, z)$ is the spatio-temporal spectrum of the laser pulse, $\hat{N}(k_x, k_y, \omega, z)$ represents the nonlinear response of the medium, $k_z(k_x, k_y, \omega) = [k^2(\omega) - k_x^2 - k_y^2]^{1/2}$ is the propagation constant, k_x , k_y , and ω are the spatial and temporal angular frequencies, μ_0 and μ are the vacuum and medium permeabilities, respectively. The nonlinear response takes into account the third order nonlinear polarization, P_{nl} , the current of free electrons J_f and the current that is responsible for ionization losses, J_a :

$$\hat{N} = \hat{P}_{nl} + \frac{i}{\omega} (\hat{J}_f + \hat{J}_a), \quad (2)$$

with

$$\hat{P}_{nl} = \varepsilon_0 \chi^3 \widehat{E^3}, \quad (3)$$

$$\hat{J}_f = \frac{q_e^2}{m_e} \frac{\nu_c + i\omega}{\nu_c^2 + \omega^2} \widehat{\rho E}, \quad (4)$$

$$\hat{J}_a = K \hbar \omega_0 \frac{\partial \widehat{\rho}}{\partial t} \frac{1}{E}, \quad (5)$$

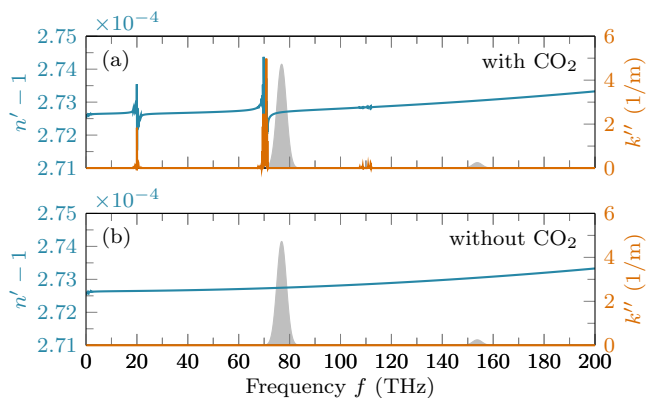


FIG. 6. The real part n' of the refractive index n (cyan) and the absorption coefficient k'' (orange) versus frequency f for air with (a) and without (b) CO_2 gas. The spectrum of the initial $3.9 \mu\text{m}$ two-color laser pulse is marked by gray.

where $\hat{}$ denotes the spatio-temporal spectrum, ε_0 is the vacuum permittivity, $\chi^3 = 4n_0^2\varepsilon_0c_0n_2/3$ is the cubic susceptibility with n_2 being the nonlinear index, n_0 is the medium refractive index at the pulse central frequency ω_0 , c_0 is the speed of light in vacuum, q_e and m_e are the charge and mass of the electron, ν_c is the collisions frequency, ρ is the concentration of free electrons (in $1/\text{m}^3$), and K is the order of the multiphoton ionization. The real part of \hat{J}_f describes inverse Bremsstrahlung, and the imaginary part is responsible for plasma defocusing.

Together with the UPPE we solve the kinetic equation for plasma concentration [24]:

$$\frac{\partial \rho}{\partial t} = R_1(\rho_{nt} - \rho) + R_2\rho, \quad (6)$$

where ρ_{nt} is the concentration of neutral molecules, with R_1 and R_2 being the optical field and avalanche ionization rates. To calculate R_1 we use the Perelomov-Popov-Terentiev (PPT) formula [28], while R_2 is given by

$$R_2 = \sigma(\omega_0) \frac{E}{U_i}, \quad (7)$$

with

$$\sigma(\omega_0) = \frac{q_e^2}{m_e} \frac{\nu_c}{\nu_c^2 + \omega_0^2},$$

being the inverse Bremsstrahlung cross-section at the pulse central frequency ω_0 , and U_i is the ionization potential. For the calculation of $\partial \rho / \partial t$ in Eq. (5) we use only the first term on the right-hand side of Eq. (6).

Real atmospheric air is a mixture of several gases, including CO_2 . One of the CO_2 absorption bands is located at $4.3 \mu\text{m}$, that is, in close proximity to the central

wavelength of our $3.9 \mu\text{m}$ pulse. In order to take into account the influence of CO_2 gas we use the following model for complex frequency-dependent refractive index of air $n = n' + in''$ [21]:

$$n(\omega) = n_{\text{Peck}}(\omega) + n_{\text{HITRAN}}(\omega). \quad (8)$$

The real valued refractive index $n_{\text{Peck}}(\omega)$ is given in [29], while to calculate the complex refractive index $n_{\text{HITRAN}} = n'_{\text{HITRAN}} + in''_{\text{HITRAN}}$ we use the data on spectral lines of atmospheric gases from the HITRAN database [26]. The imaginary part n''_{HITRAN} is recalculated from the absorption coefficient given in the database, then the real part n'_{HITRAN} is restored using the Kramers-Kronig relations. To study the influence of CO_2 resonances we calculated n_{HITRAN} for two gas mixtures that represent dry air (i.e., air with zero relative humidity): the first one with CO_2 (0.04% of CO_2 , 79.06% of N_2 , 20.9% of O_2) and the second one without CO_2 (79.1% of N_2 and 20.9% of O_2). The spectral lines for both mixtures are calculated for a temperature of 296 K and pressure of 1 atm. In Fig. 6 we plot the real part n' of the refractive index n and absorption coefficient $k'' = n''\omega/c_0$ as functions of frequency $f = \omega/2\pi$ for both gas mixtures. One can see that the presence of CO_2 gas in air gives rise to two absorption bands centered at 70 and 20 THz ($4.3 \mu\text{m}$ and $15 \mu\text{m}$, respectively). However, at this concentration of CO_2 , the highest values of the absorption coefficient k'' do not exceed several inverse meters. Therefore for our pulses focused by 200 mm lens we do not expect such strong influence of the linear absorption like in [21]. Nevertheless, the presence of CO_2 affects the sign of the second order dispersion coefficient k_2 at $\lambda_0 = 3.9 \mu\text{m}$: for the gas mixture with CO_2 the $k_2 = -8.61 \times 10^{-29} \text{ s}^2/\text{m}$ is negative and the dispersion is anomalous, while for the gas mixture without CO_2 the $k_2 = 4.18 \times 10^{-30} \text{ s}^2/\text{m}$ is positive and the dispersion is normal.

In our simulations we assume that the nonlinear index $n_2 = 10^{-23} \text{ m}^2/\text{W}$ is the same for $\lambda_0 = 0.8$ and $3.9 \mu\text{m}$ (the corresponding values of critical power P_{cr} are 9.65 and 230 GW); the concentration of neutral molecules $\rho_{nt} = 2.5 \times 10^{25} \text{ 1/m}^3$, and collision frequency $\nu_c = 5 \times 10^{12} \text{ 1/s}$. To calculate the concentration of free electrons, ρ , we assumed that air consists by 79.1% of N_2 and 20.9% of O_2 molecules with ionization potentials equal to 15.576 and 12.063 eV, respectively. For each molecule we solved a separate kinetic equation.

We solved Eq. (1) on an axially symmetric grid with the following parameters: the grid size and number of points in spatial domain are 10 mm and 1000, respectively (spatial resolution is $10 \mu\text{m}$); the grid size and number of points in time domain are 10 ps and 65536, respectively (temporal and spectral resolutions are 0.15 fs and 0.1 THz).